**Using one-dimensional waveguide resonators to measure phase velocities in bubbly liquids**

Craig N. Dolder[1] and Preston S. Wilson
Applied Research Laboratories and Department of Mechanical Engineering
The University of Texas at Austin
1 University Station C2200; Austin, Texas 78712, USA

[1]Current affiliation: Institute of Sound and Vibration Research, University of Southampton, UK; electronic mail: dolder@utexas.edu

**Abstract**

Resonator techniques can be successfully used to extract effective medium properties from dispersive materials. However, in some cases the dispersion can cause modes to repeat. If repeated modes are not taken into account the useful range of the resonator technique is limited. A resonance tube containing tethered balloons is used to create a dispersive effective medium. Resonator measurements show that modes do repeat. Direct measurement of the mode shapes allows exploitation of all longitudinal radially-symmetric modes and expands the frequency range of the technique. A theoretical model is also used to predict when modes repeat. For the presented data set this method increases the measurement range from below 160 Hz to 3000 Hz excluding the stop-band where resonances are damped. A means to account for non-ideal resonator boundary conditions often found in highly dispersive systems is discussed.

## 1 INTRODUCTION

An inhomogeneous medium can often be represented as an effective-medium with a frequency-dependent phase velocity and attenuation. Resonators are well suited for measuring the effective-medium properties of suspended scatterers in water and have been used to investigate seagrass,[1] methane hydrates,[2] microparticles,[3] freely rising bubbles,[4,5] cavitating bubbles,[6] and encapsulated bubbles[7]. Freely rising bubbles, cavitating bubbles, and encapsulated bubbles are examples of systems that can exhibit regions of negative group velocity. In a dispersive region where the group velocity is negative the wavelength of sound increases as frequency increases, which can cause mode repetition. Mode repetition refers to a single eigenmode occurring at multiple eigenfrequencies. This can also be viewed as being caused by two frequency bands with different phase speeds $c_{\mathrm{ph}}$ separated by a stop band. Group velocity is defined as

$$c_{\mathrm{gr}} = \frac{\mathrm{d}\omega}{\mathrm{d}k}, \tag{1}$$

where $k = \omega/c_{\mathrm{ph}}$ is the real part of the wavenumber, and $\omega$ is the angular frequency. In systems with attenuation the wavenumber will be complex. The complex wavenumber will be represented as $\boldsymbol{k} = \Re(\boldsymbol{k}) + i\Im(\boldsymbol{k}) = k + i\alpha$, where the imaginary component $\alpha$ is the attenuation. The convention of boldface for complex values will be used. The presence of repeated modes has either limited analysis to the low-frequency regime below any region of negative group velocity or required direct measurements of the node locations.[4,7–9] While node location measurement is common practice the concept that modes repeat has not received much attention. A method to significantly increase the upper frequency range of a resonator-based measurement is developed here. For the resonator used in this experiment the standard resonator technique resulted in a frequency range of measurements from about 80 Hz to the stop band at approximately 200 Hz, whereas the improved method results in a measurement range from the upper end of the stop band at approximately 900 Hz to 3000 Hz. Further, adjustments to improve the accuracy of the low-frequency data are presented. This article discusses experimental measurement of phase velocities above and below a region of negative group velocity and how this differs from standard modal analysis. A forward model is proposed that combines an existing model for sound propagation in a bubbly liquid with an elastic waveguide model. This allows the repetition of modes to be predicted in bubbly liquid. The elastic waveguide model is also used to predict the phase speed in free space from the resonances in the waveguide.

Effective medium sound speeds are extracted by observing the fundamental resonances of the system and relating those to the sound speed using an appropriate model. In a uniform rigid-walled waveguide of length $L$ with pressure-release end conditions (a reflection coefficient of $-1$) the wavelength $\lambda_m$ of each fundamental mode $m$ is

$$\lambda_m = \frac{2L}{m}, \tag{2}$$

which can then be used to determine the phase velocity $c_{\mathrm{ph,wg}}(f_m)$ in the waveguide at each resonance frequency $f_m$ using

$$c_{\mathrm{ph,wg}}(f_m) = \frac{2Lf_m}{m}. \tag{3}$$

To avoid confusion, the intrinsic phase velocity and wave number that would be measured from the material in the waveguide if it were in free space will be labeled without subscript $c, \boldsymbol{k}$; while the values measured in a waveguide will be given a subscript $c_{\mathrm{wg}}, \boldsymbol{k}_{\mathrm{wg}}$. It is important at this point to clarify the different families of modes that exist in the resonator. The modes are indexed according to coordinate directions. Here we are using $M$ for the radial modes, $m$, for the longitudinal modes, and $l$ for variations in the circumferential direction. Any mode in the system can be identified by its modal coordinates $(M, l, m)$. For a rigid waveguide the family of modes where $M = 0$ and $l = 0$ refer to modes with no variation in the radial or circumferential directions. These modes have no cut-off frequency and the phase velocity in the waveguide and the sound speed in free space would be equal. Sections II and III of this paper use these modes to evaluate the phase velocity and will

index the modes solely in terms of $m$. In the real system there will be a variation in the radial direction and the phase velocity will vary from the free space sound speed.

Equation (3) is taken as a starting point for the corrections discussed. For a fill-material with no region of negative group velocity, Eq. (3) is used to find the phase speed of the material in the waveguide. The sound speed in the waveguide is calculated by identifying the radially symmetric resonances of the system and then relating those resonances to their respective modes. The modes are generally clearly identifiable and can be assumed to progress in ascending order, $m = \{1, 2, 3, \ldots\}$. Then a correction is made for the elastic waveguide effect. For the $M = 0$, $l = 0$ family of modes (this corresponds to the mode defined as ET0 in Ref. 10) the introduction of an elastic wall reduces the sound speed within the waveguide relative the free field value. Another mode that can propagate down to zero frequency also exists and is supersonic with respect to the material in the waveguide, but for the frequencies investigated this mode is believed to consist primarily of a plane wave in the wall that is coupled to the liquid through the radial motion at the wall-liquid interface.[10] The elastic waveguide's effect on the phase speed has been addressed by Del Grosso[11] and appropriate models have been used to either minimize the effect[12] or accept the effect and correct the measured sound speed[13–15].

The experimental design is discussed in Sec. II. The identification of modes and mode repetition is discussed in Sec. III. Further, any system with significant dispersion is likely to exhibit a complex reflection coefficient at the resonator boundary. If the reflection coefficient is complex then neither a node nor an antinode occurs at the boundary. If the material properties are being calculated from the node positions, precise knowledge of those locations are necessary. The resultant shift of the nodes away from the boundary changes the standing wave pattern and requires modification of Eq. (3), which is discussed in Sec. IV. The nodal shift is similar to the canonical problem of the end correction for a resonance tube and is discussed both in terms of arbitrary impedance and then applied to bubbly liquids.

## 2 EXPERIMENT

The resonator needed to be large enough to scan the internal pressure field with sufficient resolution to determine the mode shapes. It was a constructed from an aluminum pipe that was 1.985 m long, had an outer radius of 0.1085 m and a wall thickness of 7 mm. A schematic of the experimental arrangement is shown in Fig. 1. The bottom of the tube had a thin rubber membrane which was supported by a layer of expanded polystyrene foam 12.2 cm thick. The linear sweep source signal was generated using LabView software and output by an NI PCI 4461 data acquisition module. The signal was amplified by a Crown audio power amplifier that drove a Labworks ET-126HF-1 shaker. The shaker was suspended above the top surface of the resonator on a resilient support made of closed-cell foam resting on the top rim of the resonator. The shaker had a 38.1 mm diameter piston that was submerged 30 mm below the air-water interface. The piston had a slight convex curve in order to prevent bubbles from adhering to it. A Reson model TC4013 hydrophone was used to scan the sound field in the resonator. It was attached to a linear rail and moved by a stepper motor controlled by the PC software. The hydrophone signal was amplified by a Brüel and Kjær Nexus charge amplifier and recorded by the NI PCI 4461 module.

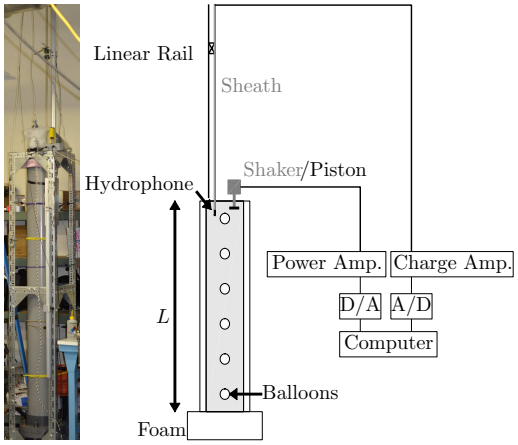


**Figure 1:** (Color online) (Left) Picture of the aluminum pipe resonator apparatus. (Right) Schematic of the resonator showing six submerged balloons, a shaker-driven piston for acoustic excitation, and a hydrophone mounted on a linear traverse for mapping the modal structure of the acoustic field.

The pipe was filled with water. The water in the resonator was raised to approximately 40 degrees Celsius, stirred and tapped to cause any bubbles on the walls to rise, and then allow to settle to 30.4 degrees Celsius. This was done to decrease the dissolved gas content of the resonator and to eliminate any unwanted bubbles. The temperature did not change more than 0.2 degrees Celsius during the experiment and the sound speed[16] and density[17] used in the analysis were taken from tabulated values for pure degassed water at this temperature. Air-filled Qualatex balloons that deviated slightly from a spherical shape were used. Small variations from spherical conditions are not believed to significantly affect the bubble res-

onance[18] since a prolate spheroid of aspect ratio of 1.414 only varies in resonance frequency and damping from a spherical bubble by less that 1%.[19] The volume of each balloon was measured through the water it displaced when submerged, then the equivalent spherical radius was determined as the radius that would displace the same volume of water. Six balloons with equivalent spherical radii of 2 cm were attached to a monofilament nylon line so that there was an $L/6$ distance between each balloon and an $L/12$ distance between each end balloon and a termination, where $L$ is the length of the water column in the pipe. From a metamaterials perspective this would equate to six segments of water each with a balloon at the center. A pulley attached at the bottom of the tube was used to lower the balloons into the resonator. This system had the material properties shown in Tab. I. The values that define the waveguide are the sound speed and density of water without bubbles ($c_1$ and $\rho_1$ respectively), the compressional and shear wave speeds of the wall material ($c_\mathrm{c}$ and $c_\mathrm{s}$ respectively), the density of the wall material ($\rho_\mathrm{w}$), the sound speed and density of the foam layer ($c_\mathrm{foam}$ and $\rho_\mathrm{foam}$), the sound speed and density of the floor ($c_\mathrm{floor}$ and $\rho_\mathrm{floor}$), the inner and outer radii of the pipe ($b$ and $d$), and the length of the foam layer ($l$). The parameters used to define the effective medium are the shear modulus, density, viscosity, and thickness of the balloon shell material ($G$, $\rho_\mathrm{s}$, $\mu$, and $t$ respectively), the number of balloons ($N$), and the inner radius of the bubbles ($r$). In terms of practical application the bubble radius, number of bubbles, and volume of the pipe can be used to calculate the probability density function of bubble size and volume fraction of air. The probability density function $f(r)$ is a dirac-delta located at $r = 0.02$ since the population is mono-disperse. The volume fraction of air was $\chi = 0.00337$. The shear modulus of the balloon shells was a free parameter with no direct method of measurement. In addition evidence suggests that the elastic and shear moduli vary nonlinearly with the amount of inflation.[20,21] Therefore the only method of determining the shear modulus available for this study was to use it as a fitting parameter with the model. The shear modulus was determined by finding value of $G$ that minimized the mean-squared error between the model and the data for the first four resonances. The value used was found to be within the uncertainty for natural rubber.[22] The shear viscosity of the shell material was chosen to be within the possible range for latex rubber, however using any value from 0.0 - 50 Pa s has no impact on the results. For balloons of this size the effect of surface tension is negligable and was omitted by setting the surface tension terms to zero. The physical parameters of the resonator wall material were verified by measuring the system sound speed while filled with degassed water.

| Resonator parameters | | |
|---|---|---|
| Sound speeds [m/s] | Densities [kg/m$^3$] | Dimensions [m] |
| $c_1 = 1510$ | $\rho_1 = 995.5$ | $b = 0.1015$ |
| $c_\mathrm{c} = 6420$ | $\rho_\mathrm{w} = 2700$ | $d = 0.1085$ |
| $c_\mathrm{s} = 3205$ | $\rho_\mathrm{air} = 1.21$ | $L = 1.844$ |
| $c_\mathrm{foam} = 717$ | $\rho_\mathrm{foam} = 29$ | $l = 0.1220$ |
| $c_\mathrm{floor} = 3100$ | $\rho_\mathrm{floor} = 2600$ | |
| Effective medium parameters | | |
| $G = 2.02 \times 10^6$ Pa | $\rho_\mathrm{s} = 930\,\mathrm{kg/m^3}$ | $r = 0.02$ m |
| $\mu = 5$ Pa s | $N = 6$ | $t = 0.000\,08$ m |
| $D = 2.207 \times 10^{-5}\,\mathrm{m^2/s}$ | $\gamma = 1.40$ | |

**Table I:** Parameters for the resonator and effective medium discussed in Secs. III and IV.

## 3 IDENTIFICATION OF LONGITUDINAL MODES

Mode identification can be approached by considering the system as a three-medium plane-wave propagation problem where a plane wave originates in a material with an acoustical impedance $Z_1$, passes through the fill material with impedance $Z_\mathrm{fill}$, then a wave is transmitted into another medium on the far side with impedance $Z_2$, as shown in Fig. 2. According to ideal theory, as long as all of the acoustic impedances are real, $Z_1 < Z_\mathrm{fill}$, and $Z_2 < Z_\mathrm{fill}$, pressure minima will occur at the interfaces and the standing wave pattern inside the resonator evolves with the addition of one half-wavelength inside the tube each time the mode number increases. In practice the minima are expected to occur near the interfaces only if $Z_1$ and $Z_2$ are both significantly smaller than $Z_\mathrm{fill}$.

| $Z_1$ | $Z_\mathrm{fill}$ | $Z_2$ |
|---|---|---|

**Figure 2:** Illustration of the impedances ($Z_1$, $Z_\mathrm{fill}$, $Z_2$) in a three medium problem, where acoustic plane waves would be propagating from left to right.

It is also generally expected that each resonance frequency of the system has a unique mode shape. Consider the measurements from this study shown in Fig. 3. They show the relative acoustic pressure at one position within a bubbly-liquid filled resonator including the frequency range of individual bubble resonance. This response would be interpreted as consisting of four fundamental modes corresponding to one through four half-wavelengths filling the resonator, then a high attenuation region in which resonances are damped out, and then some higher-order modes appearing around 900 Hz. The gap in the harmonic modal structure between 200 Hz and 900 Hz makes it impossible to interpret the modes above 900 Hz, and with no other information, there is no way to unambiguously relate the resonances above

900 Hz to the sound speed. Knowledge of the mode shapes allow the appropriate modes to be identified and reveals the unusual phenomenon of mode repetition.

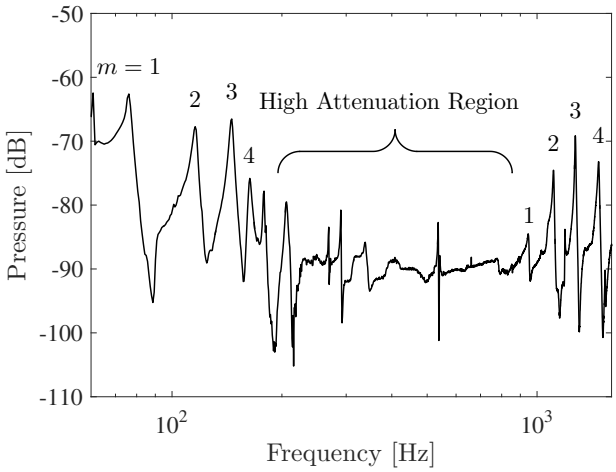


**Figure 3:** Example spectrum from a water-filled resonator with 6 elastic-shelled air bubbles present. The first four fundamental modes repeat above the high attenuation region because of negative group velocity in the high attenuation region. The dB scale represents relative acoustic pressure.

The acoustic pressure measured within the resonator at 102 lengthwise positions is shown in Fig. 4, where the dashed line represents the location of the spectrum shown in Fig. 3. The first resonance above the high attenuation region is a repeated $m = 1$ mode (a single half-wavelength fills the resonator), and the progression repeats as seen in the lower frequency range. The corresponding modes between 900 Hz and 1.5 kHz are $m = 1, 2, 3$, and 4, as shown in Fig. 3.

We can model the effect of repeating modes by replacing the real acoustic impedances in the three medium problem with appropriate complex acoustic impedances. First we need the sound speed $\boldsymbol{c}$ and density $\rho$ of the fill material in free space. For encapsulated bubbles we use Church's model[23] to obtain the complex sound speed $\boldsymbol{c}$.

$$\frac{c_1^2}{\boldsymbol{c}^2} = 1 + \frac{4\pi c_1^2 \rho_1}{\alpha_c \rho_s} \int_0^\infty \frac{r f(r)\, \mathrm{d}r}{\omega_0^2 - \omega^2 + j\omega\delta}, \qquad (4)$$

where $c_1$ and $\rho_1$ are the sound speed and density of water without bubbles, $r$ is the inner radius of the bubble shell, $\alpha_c = [1 + (r/(r+t))(\rho_1 - \rho_s)/\rho_s]$, $f(r)$ is the probability density function of bubble size, $t$ is the thickness of the shell, and $\omega_0$ is a frequency dependent resonance frequency

$$\omega_0 = (\rho_s r^2 \alpha_c)^{-1} \left\{ 3\kappa P_0 - \frac{2\sigma_1}{r} - \frac{2\sigma_2 r^3}{(r+t)^4} + 4\frac{V_s G_s}{(r+t)^3}\left[1 + Z_c\left(1 + \frac{3r^3}{(r+t)^3}\right)\right]\right\}, \qquad (5)$$

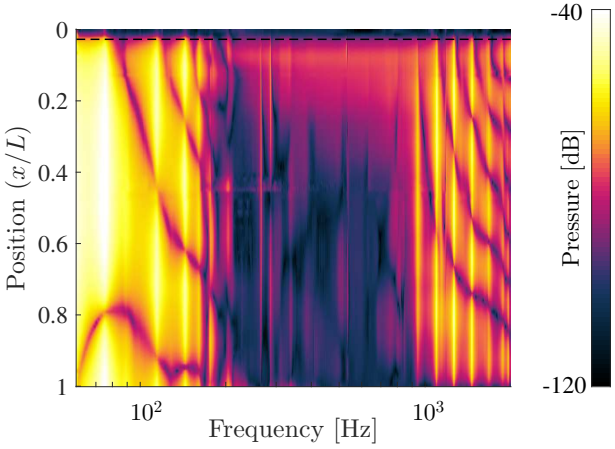


**Figure 4:** (Color online) An example spectra from a water-filled resonator with 6 elastic-shelled air bubbles present. The dashed line represents the spectrum shown in Fig. 3. The origin is located at the air-water interface.

where $\sigma_1$ is the surface tension on the inner interface of the shell, $\sigma_2$ is the surface tension on the outer interface of the shell, $P_0$ is the static pressure outside the bubble, $V_s = (r+t)^3 - r^3$ , $Z_c$ is defined by

$$Z_c = \left[\frac{2\sigma_1}{r} + \frac{2\sigma_2}{(r+t)}\right]\left[\frac{(r+t)^3}{V_s}\right](4G_s)^{-1}, \qquad (6)$$

and $\kappa = \Re(\Phi)/3$ is an effective polytropic exponent of the gas. The term $\Phi$ comes from thermodynamic relations of the bubble's volume oscillations[24] and is defined as

$$\Phi = \frac{3\gamma}{1 - 3(\gamma-1)i\chi_c[(i/\chi_c)^{1/2}\coth((i/\chi_c)^{1/2}) - 1]}, \qquad (7)$$

where $\gamma$ is the gas ratio of specific heats, $\chi_c = D/(\omega r^2)$, and $D$ is the gas thermal diffusivity.

For the meaurements presented in the paper the collection of balloons is mono-disperse, therefore $f(r)$ is a delta function located at $r = 0.02$ m The complete set of equations provides a solution in terms of

$c_1$, $\rho_1$, $r$, $t$, the volume fraction of air $\chi$, the gas ratio of specific heats $\gamma$, the gas thermal diffusivity $D$, the shell shear modulus $G$, the shell density $\rho_s$, the shell viscosity $\mu$, and the viscosity of water $\mu_l$. For bubbles of this size the surface tension does not play a significant role so both the surface tension at the gas-shell interface and the shell-liquid interface were considered to be zero. The value for the damping coefficient $\delta$ contains terms to account for four different damping mechanisms

$$\delta = \underbrace{\frac{4r\mu_l}{(r+t)^3\rho_s\alpha_c}}_{\text{viscous liquid}} + \underbrace{\frac{4V_s\mu_s}{(r+t)^3r^2\rho_s\alpha_c}}_{\text{viscous shell}} + \underbrace{\frac{4\mu_{th}}{r^2\rho_s\alpha_c}}_{\text{thermal}} + \underbrace{\frac{\omega^2(r+t)}{c_1(1+(\omega(r+t)/c_1)^2)}}_{\text{acoustic}}, \quad (8)$$

where $\mu_{th} = P_0\Im[\Phi]/(4\omega)$ is an effective thermal viscosity.[25]

The complex wavenumber of the system is $\boldsymbol{k} = \omega/\boldsymbol{c}$, the phase velocity is $c_{ph} = \omega/\Re[\boldsymbol{k}]$, and the attenuation coefficient is $\alpha = \Im[\boldsymbol{k}]$. The instance of multiple resonances for the same modal shape can be predicted by looking at the $k-\omega$ plot of the system. Equation (3) can be rearranged to solve for $kL$ to give

$$kL = \pi m. \quad (9)$$

Each time Eqn. 9 is satisfied, the $m^{th}$ resonance occurs. Since $\pi m$ is real we match the condition to the real part of the wavenumber. The bubbly-liquid case mentioned earlier had the parameters listed in Tab. I. The $k-\omega$ plot is shown in Fig. 5, where the real part of the wavenumber is shown on the right and the imaginary part of the wavenumber is shown on the left. The plot would appear to indicate that each resonance occurs three times; however, when the slope of the $k-\omega$ plot is negative the group velocity is negative. The negative group velocity occurs in a stop band, therefore no resonances occur in that region. The beginning and end of the stop band is determined by setting $\delta$ in Eq. (4) to zero and determining when the wavenumber is entirely imaginary. If scanning the length of the resonator with a hydrophone is not feasible a forward model can be used to predict the approximate node locations and mode numbers.

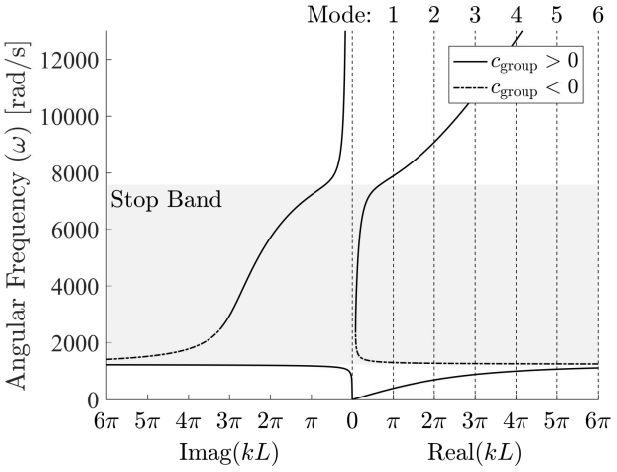


**Figure 5:** A $k-\omega$ plot for a bubbly-liquid fill material. The vertical dashed lines represent each mode and each mode is present when the dashed line crosses the solid line, except for the region around $\omega \approx 1270$ rad/s, where the group velocity is negative.

When considering the physical phenomenon of repeating modes in bubbly liquid there are at least two distinct ways to visualize what happens. The first is to consider that the low-frequency limit of a bubbly liquid is considered to act like an effective medium where the densities are averaged and the stiffnesses add in parallel.[26] In the high frequency limit the bubbles appear acoustically rigid and the sound speed approaches that of bubble free water. Between these two limits is a stop-band. Therefore according to this mindset you are seeing the resonances for each regieme on the opposing sides of the stop band. This is illustrated in Fig. 6. A refinement of this view is acheived when the damping term Eq. (8) is set to zero in Eq. (4), which is also illustrated in Fig. 6. Here the low-frequency phase velocity tends toward zero as frequency increases, then there is a stop band, and then there is an asymptote with infinite phase speed at the upper end of the stop-band that trends toward the high-frequency limit. When a real system with finite damping is considered these two regions stitch together to make the phase speed continuous. Experimental measurements by Cheyne *et al*[4] reveal that phase speeds can be measured in the stop band and they bridge the two regions. It is in this region where theoretically a region of negative group velocity exists where the wavelength increases with frequency. An alternate view is that the presence of regions of negative group velocity can cause modes to cease progression in monotonically ascending order and can cause modes to repeat. This study did not measure any velocities in this region. Regardless of the viewpoint, once the repeated modes are accounted for the phase speed can be correctly determined.

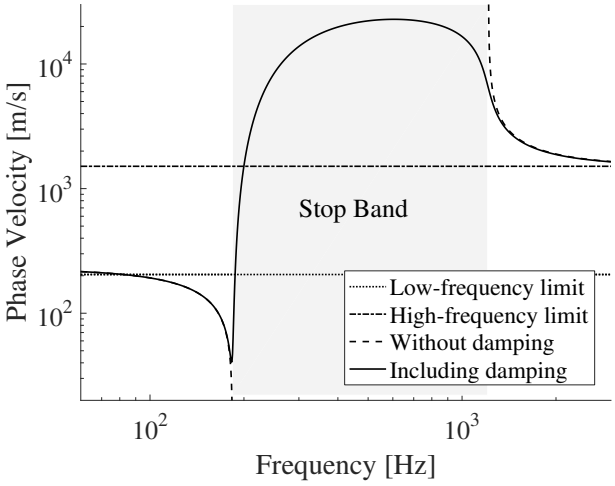


**Figure 6:** The phase velocity can be thought of as two regions separated by a stop-band with different limits or a continuous function with a region where the wavelength increases as frequency increases. If damping is not included in the bubbly liquid model the phase velocity starts at a low-frequency effective medium limit and goes to zero at bubble resonance. After the stop band the phase velocity starts from a vertical asymptote of positive infinity and approaches a high-frequency effective medium limit. These different limits can cause modes to occur more than once.

The next step in relating the observed and identified resonance frequencies to the intrinsic phase velocity of the fill material is to account for the elastic walls of the waveguide. Del Grosso[11] derived expressions for the axially symmetric velocity potentials in an elastic tube and a fluid core that were coupled through the radial motion at the inner radius $b$, of the elastic tube. The additional boundary conditions were that the tangential stress vanishes at the inner radius and the outer radius $d$, of the elastic tube, and the equality of negative pressure to radial stress at both boundaries. The derivation later goes on to assume the external liquid vanishes (pressure release condition). By applying the boundary conditions to velocity potentials in the wall and liquid a set of equations is obtained, the solution of which must have a determinant of zero. The expression of the determinant in the form of Eq. (5) of the revisited derivation by Lafleur and Shields,[10] was used and requires the phase velocity of the fill material in the waveguide $c_{\mathrm{ph,wg}}$, the phase velocity of the fill material in free space $c$, the density of the material in the waveguide $\rho = \rho_1(1-\chi) + \rho_{\mathrm{air}}\chi$, the compressional and shear wave speeds of the wall material $c_{\mathrm{c}}$ and $c_{\mathrm{s}}$ respectively, and the angular frequency $\omega$. The determinant cannot be solved analytically for either the phase velocity of the fill material in the waveguide or the phase velocity of the fill material in free space, but given either parameter the other can be found numerically.

The wavenumber in the waveguide $\boldsymbol{k}_{\mathrm{wg}}$ is considered to be the combination of the real wavenumber computed from the phase velocity in the waveguide $k = \omega/c_{\mathrm{wg}}$ and the attenuation from the bubbly liquid model $\alpha = \Im[\omega/\boldsymbol{c}]$,

$$\boldsymbol{k}_{\mathrm{wg}} = \frac{\omega}{c_{\mathrm{ph,wg}}} - j\alpha. \tag{10}$$

To summarize, the forward model consists of determining the phase velocity $c_{\mathrm{ph}}$ and the attenuation in bubbly liquid. The phase velocity is then used as an input to an elastic waveguide model to produce the phase velocity in the waveguide $c_{\mathrm{ph,wg}}$. Then the attenuation from the bubbly liquid model and the phase velocity from the elastic waveguide model are used to determine the complex wavenumber in the waveguide $\boldsymbol{k}_{\mathrm{wg}}$. In this low-frequency, low-attenuation, region of the elastic waveguide model, using the attenuation from free space is not believed to introduce significant error and this simplification significantly reduces the computation complexity. The model does have limitations. As the phase velocity of the liquid in the waveguide is increased the system phase velocity approaches a maximum phase speed. If the experimental phase velocity is higher than this maximum system phase velocity then an inversion from system phase velocity to free space phase velocity is not possible.

## 4 TERMINATION BOUNDARY CONDITIONS

For a water filled waveguide with a free air surface the approximation of a pressure-release condition is appropriate. At a temperature of 20° C and an absolute pressure of $1.013 \times 10^5$ Pa the plane-wave reflection coefficient is:

$$R = \frac{Z_{\mathrm{end}} - Z}{Z_{\mathrm{end}} + Z} = \frac{415 - 1.48 \times 10^6}{415 + 1.48 \times 10^6} = -0.9994, \tag{11}$$

where $Z_{\mathrm{end}}$ is the characteristic impedance seen at the end of the resonator (approximated by a plane wave propagating in air) and $Z$ is the characteristic impedance of the fill material. The difference in impedances is so large that even if the fill material had a complex impedance, the resulting reflection will be close to -1 and have only a very small complex component.

For a vertically oriented resonator, an air-water interface is easy to maintain on the upper end; however, because of gravity it is not possible at the other end. An adequate substitute is often closed cell foam.

Lacking any way to have an ideal boundary at the lower end, closed-cell foam was cut to have a circular cross section slightly larger than the pipe and placed underneath the tube to support the thin rubber membrane that held the water. It was hoped that this would prevent the sound field from coupling into the floor, however modeling and experimental data showed that it was insufficient at low frequencies. The closed-cell foam used in this discussion has an acoustic impedance of $2.08 \times 10^4$ Rayl as determined by measuring the mass, volume, and sound speed of samples. The sound speed was determined by measuring the pulse time of flight across sheets of the foam. As discussed at the beginning of Sec. II, if all impedances are real and the fill material has the highest impedance, pressure minima occur at the terminations. If either the acoustic medium within the resonator or the termination at the lower end of the resonator has a complex acoustic impedance, a pressure minimum does not occur at the termination. Instead the node shifts away from the termination. The fill material will have a complex acoustic impedance if it is dispersive or has attenuation and the boundary condition at the termination will be complex if the termination deviates from anything other than an ideal, infinite half space. In this case neither the foam layer nor the floor could be considered to have 1-D propagation, but it was considered a sufficient approximation. While the nodal shift may be small enough to be neglected in many cases, an expression for the nodal shift can be used to predict the error in assuming a node at the termination. The reflection coefficient $\boldsymbol{R}$ of any termination can be expressed as:

$$\boldsymbol{R} = \phi e^{j\psi}, \tag{12}$$

where $\phi = |\boldsymbol{R}|$ is the amplitude of the reflection coefficient and $\psi$ is the phase angle. The phase angle can be related to the distance of the pressure minima $d_{\min,n}$ from the termination through the relation:

$$kd_{\min,n} = \frac{1}{2}\psi - \frac{1}{2}\pi - n\pi, \tag{13}$$

where $k$ is the wave number of the fill material in the waveguide and $n$ is a non-negative integer. For example, consider a water-filled resonator tube with rigid walls that is terminated by closed cell foam of thickness $l$ and an acoustic impedance of $Z_{\text{foam}} = 2.08 \times 10^4$ Rayl that is on a concrete floor with an acoustic impedance of $Z_{\text{floor}} = 8.06 \times 10^6$ Rayl.[27] Since the concrete floor had an unknown finite thickness and the acoustic impedance of concrete can vary it is acknowledged that there was no way for the model to exactly match the physical system. The local impedance at the termination of the resonator can be found using the impedance translation theorem[28]

$$\boldsymbol{Z}_{\text{end}} = Z_{\text{foam}} \frac{Z_{\text{floor}} \cos(k_{\text{foam}} l) - jZ_{\text{foam}} \sin(k_{\text{foam}} l)}{Z_{\text{foam}} \cos(k_{\text{foam}} l) - jZ_{\text{floor}} \sin(k_{\text{foam}} l)}, \tag{14}$$

where $k_{\text{foam}}$ is the wave number in the closed cell foam layer. Even if the medium in the resonator is non-dispersive, the complex termination impedance will cause the pressure minima to depart from the termination. The distance of this variation can be calculated using Eqs. (11) through (14) for an elastic-walled, resonator with tethered balloons and the same length and sound speed properties listed in Tab. I and is shown in Fig. 7. Another interesting phenomena to observe is that at around 2900 Hz there is a pressure maximum at the interface due to a half wavelength standing wave in the foam layer.

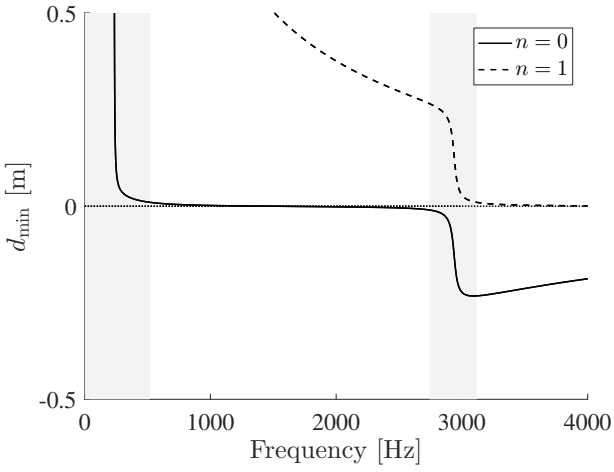


**Figure 7:** Distance of pressure minimum from boundary. In shaded regions the pressure minimum is more than 1 cm from the boundary. Although the boundary is acoustically softer than the contents of the waveguide, nodes depart from the boundary at low frequencies and around resonances of the foam layer.

There are two ways to compensate for this condition. The first is to compensate the phase speed calculation using a measurement of the distance, $x$, between the lowest node and the upper boundary. The second is to use the relation for nodal shift to adjust the phase speed. This second method, however, requires either a model that represents the system well or iterative solution involving both the sound speed and attenuation.

Given direct knowledge of the node location, the phase speed $c_{\text{ph,wg}}$ can be determined as:

$$c_{\text{ph,wg}} = \frac{2Lf}{q}\bar{x}, \tag{15}$$

where $q$ is the number of half wavelengths between the air/water interface and the node at $\bar{x} = x/L$. Many times it is not possible to measure the pressure field along the length of the resonator, but a correction is still possible if there is a sufficient model for the medium in the resonator and the impedance of the interface is well known through the relation:

$$c_{\mathrm{ph,wg}} = \frac{2(L + d_{\mathrm{min}})f}{n}, \tag{16}$$

where $d_{\mathrm{min}}$ is the closest pressure minimum to the end of the resonator as determined by Eq. (13). Note that $d_{\mathrm{min}}$ will be negative if the node has shifted into the resonator.

For example, a model for the dispersion through elastic-shelled bubbles can provide an approximation for the acoustic impedance of the medium, which can be used to predict the change in the position of the nodes. The acoustic field measurements shown in Fig. 4 and described in Sec. II are replotted in Fig. 8 to emphasize the frequency range below 200 Hz. The first four modes are labeled and the nodal deviations away from the boundary can be easily seen. Fig. 9 shows the phase speed calculated from the spectra if a) no nodal shift is not taken into account b) if Eq. (15) is used given the location of the last node, and c) if Eq. (16) is used to estimate the correction. It is important to note that Eq. (16) can only be used if there is a reasonable estimate for the acoustic impedances of both the termination and the medium under test. Here the system is well modeled and both corrections adjust the sound speed to within 10 m/s of the prediction for the resonances below the individual bubble resonance frequency. Above the individual bubble resonance frequency free medium sound speeds are calculated for modes four through eleven. No correction for the measured node location is presented for this range because the node shifts beyond the boundary. The sound speeds for the repeat modes one through three could not be calculated due to the artificial maximum sound speed introduced by elastic waveguide model as discussed at the end of Sec. III.

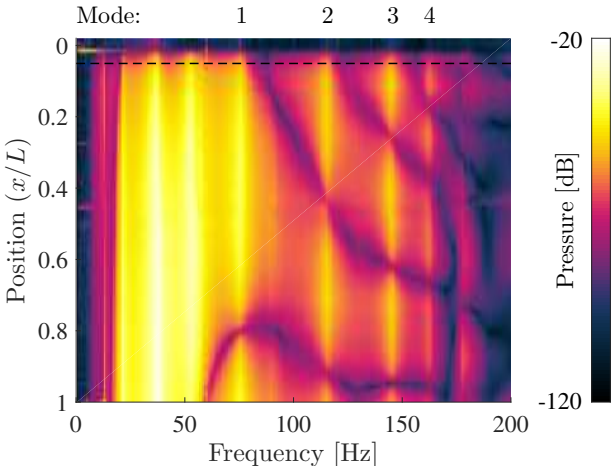


**Figure 8:** (Color online) Example spectra from a water-filled resonator with 6 elastic-shelled air bubbles present focused on the low-frequency region. The dashed line represents the spectrum shown in Fig. 3. The origin is located at the air-water interface.

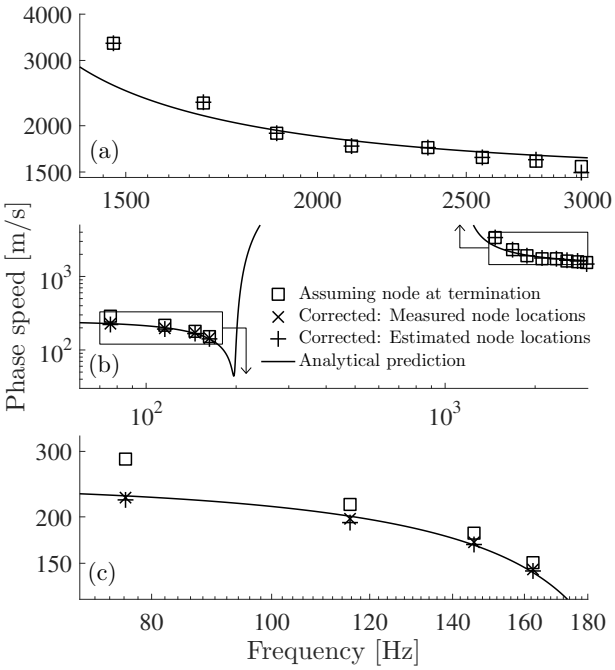


**Figure 9:** Phase speeds estimated using different assumptions regarding the node locations compared to the analytical prediction of the Church model. (a) The resonances above the individual bubble resonance frequency. Shown here are modes 4 through 11. Note that a correction due to the measured node locations was not possible because the node shifts beyond the boundary at these frequencies. (b) The entire frequency range. (c) The low-frequency resonances below the individual bubble resonance frequency.

## 5 CONCLUSIONS

Improvements in the understanding of errors associated with the use of water filled resonators exhibiting negative group velocity were discussed and corrections presented. It is important to determine the modal shape of each resonance as mode shapes can repeat when highly dispersive fill materials are studied. Two methods can be used to utilize repeated modes in the analysis. A pressure sensor can be used to scan the system to determine the mode shapes experimentally. Alternatively when scanning with a sensor is not possible a forward model that predicts the phase velocity and attenuation through bubbly liquid can be used,the phase velocity can be compensated for the presence of an elastic cylindrical shell and the location and mode numbers and frequencies can be estimated. Once the mode numbers are identified the experimental resonances can be used to compute phase velocities. Both experimental measurement of the mode shapes and the use of a forward model allowed the modes above the individual bubble resonance frequency to be utilized.

When using closed-cell foams to approximate a pressure-release boundary condition, either standing waves in the foam layer or the dispersive nature of the fill material can cause nodes to shift away from the termination. The change in wavelength associated with the nodes shifting away from the termination can be corrected similarly by either scanning the effective medium to locate the last node of each resonance or using a forward model to estimate the change in the node locations.

### Acknowledgments

The authors acknowledge support of the Office of Naval Research and the Applied Research Laboratories at The University of Texas at Austin. The authors also wish to thank T. G. Leighton for useful discussions about the material.

### References

1. C. J. Wilson, P. S. Wilson, and K. H. Dunton, "Assessing the low frequency acoustic characteristics of *Macrocystis pyrifera*, *Egregia menziessi*, and *Laminaria solidungula*," J. Acoust. Soc. Am. **133**, 3819–3826 (2013).
2. C. A. Greene, P. S. Wilson, and R. B. Coffin, "Acoustic determination of methane hydrate dissociation pressures," in *7th International Conference on Gas Hydrates (ICGH 2011)*, 1–11 (2011).
3. L. Ostrovsky, "Concentration of microparticles and bubbles in standing waves," J. Acoust. Soc. Am. **138**, 3607–3612 (2015).
4. S. A. Cheyne, C. T. Stebbings, and R. A. Ray, "Phase velocity measurements in bubbly liquids using a fiber optic laser interferometer," J. Acoust. Soc. Am. **97**, 1621–1624 (1995).
5. D. M. Farmer, S. Vagle, and D. Booth, "Reverberation effects in acoustical resonators used for bubble measurements," J. Acoust. Soc. Am. **118**, 2945–2960 (2005).
6. P. R. Birkin, T. G. Leighton, J. F. Power, M. D. Simpson, A. M. L. Vinçotte, and P. F. Joseph, "Experimental and theoretical characterization of sonochemical cells. part 1. cylindrical reactors and their use to calculate the speed of sound in aqueous solutions," J. Phys. Chem. A **107**, 306–320 (2003).
7. K. M. Lee, K. T. Hinojosa, M. S. Wochner, T. F. Argo, P. S. Wilson, and R. S. Mercier, "Sound propagation in water containing large tethered spherical encapsulated gas bubbles with resonance frequencies in the 50 Hz to 100 Hz range," J. Acoust. Soc. Am. **130**, 3325–3332 (2011).
8. E. Silberman, "Sound velocity and attenuation in bubbly mixtures measured in standing wave tubes," J. Acoust. Soc. Am. **29**, 925–933 (1957).
9. R. E. Henrey, M. A. Grolmes, and H. K. Fauske, "Pressure-pulse propagation in two-phase one- and two-component mixtures, ANL-7792," Argonne National Lab. (1971).
10. L. D. Lafleur and F. D. Shields, "Low-frequency propagation modes in a liquid-filled elastic tube waveguide," J. Acoust. Soc. Am. **97**, 1435–1445 (1995).
11. V. A. Del Grosso, "Analysis of multimode acoustic propagation in liquid cylinders with realistic boundary conditions - application to sound speed and absorption measurements," Acta Acust. united Ac. **24**, 299–311 (1971).
12. P. S. Wilson, R. A. Roy, and W. M. Carey, "An improved water-filled impedance tube," J. Acoust. Soc. Am. **113**, 3245–3252 (2003).
13. P. S. Wilson, A. H. Reed, J. C. Wilbur, and R. A. Roy, "Evidence of dispersion in an artificial water-saturated sand sediment," J. Acoust. Soc. Am. **121**, 824–832 (2007).
14. K. Baik, J. Jiang, and T. G. Leighton, "Acoustic attenuation, phase and group velocities in liquid-filled pipes: Theory, experiment, and examples of water and mercury," J. Acoust. Soc. Am. **128**, 2610–2624 (2010).
15. T. G. Leighton, K. Baik, and J. Jiang, "The use of acoustic inversion to estimate the bubble size distribution in pipelines," Proc. R. Soc. A **468**, 2461–2484 (2012).
16. C. Chen and F. J. Millero, "Speed of sound in seawater at high pressures," J. Acoust. Soc. Am. **62**, 1129–1135 (1977).
17. M. Tanaka and G. Girard and R. Davis and A. Peuto and N. Bignell, "Recommended table for the density of water between 0 °C and 40 °C based on recent experimental reports," J. Acoust. Soc. Am. **38**, 301–309 (2001).
18. M. Minnaert, "On musical air-bubbles and the sounds of running water," Lond. Edinb. Dublin Philos. Mag. **16**, 235–248 (1933).
19. C. Feuillade and M. F. Werby, "Resonances of deformed gas bubbles in liquids," J. Acoust. Soc. Am. **96**, 3684–3692 (1994).
20. W. A. Osborne and W. Sutherland, "The elasticity of rubber balloons and hollow viscera," Proc. Roy. Soc. B **81**, 485–499 (1909).
21. E. Verron and G. Marckmann, "Numerical analysis of rubber balloons," Thin Wall Struct. **41**, 731–746 (2003).
22. A. R. Payne and J. R. Scott, "Properties of vulcanised natural and synthetic rubbers," in *Engineering design with rubber* (Mclaren, London, 1960), App. 3, pp. 243–247.
23. C. C. Church, "The effects of elastic solid surface layer on the radial pulsations of gas bubbles," J. Acoust. Soc. Am. **97**, 1510–1521 (1995).
24. K. W. Commander, and A. Prosperetti, "Linear pressure waves in bubbly liquids: Comparison between theory and experiments," J. Acoust. Soc. Am. **85**, 732–746 (1989).
25. A. Prosperetti, L. A. Crum and K. W. Commander "Nonlinear bubble dynamics," J. Acoust. Soc. Am. **83**, 502–514 (1988).
26. Mallock, A., "The Damping of Sound by Frothy Liquids," Proc. Roy. Soc. A **84**, 391–395 (1910).
27. D. T. Blackstock, "Elastic constants, velocity of sound, and characteristic impedance," in *Fundamentals of Physical Acoustics* (John Wiley & Sons, Inc., New York, 2000), App. A, pp. 510–512.
28. A. D. Pierce, "Multilayer transmission and reflection," in *Acoustics* (Acoust. Soc. Am., Melville, NY, 1994), Chap. 3, pp. 137–140.